Rapid Communications

Origin of diverse nematic orders in Fe-based superconductors: 45° rotated nematicity in AFe$_2$As$_2$ (A=Cs, Rb)

Seiichiro Onari and Hiroshi Kontani
Department of Physics, Nagoya University, Furo-cho, Nagoya 464-8602, Japan

(Received 23 September 2018; revised manuscript received 21 May 2019; published 29 July 2019)

The origin of diverse nematicity and their order parameters in Fe-based superconductors have been attracting increasing attention. Recently, a new type of nematic order has been discovered in heavily hole-doped ($n_d = 5.5$) compound AFe$_2$As$_2$ (A = Cs, Rb). The discovered nematicity has B_{2g} ($=d_{xy}$) symmetry, rotated by 45° from the B_{1g} ($=d_{x^2-y^2}$) nematicity in usual compounds with $n_d \approx 6$. We predict that the "nematic bond order," which is the symmetry breaking of the correlated hopping, is responsible for the B_{2g} nematic order in AFe$_2$As$_2$. The Dirac pockets in AFe$_2$As$_2$ is essential to stabilize the B_{2g} bond order. Both B_{1g} and B_{2g} nematicity in A_{1-x}Ba$_x$Fe$_2$As$_2$ are naturally induced by the Aslamazov-Larkin many-body process, which describes the spin-fluctuation-driven charge instability. The present study gives a great hint to control the nature of charge nematicity by modifying the orbital character and the topology of the Fermi surface.

DOI: 10.1103/PhysRevB.100.020507

The electronic nematic state, which is the spontaneous rotational symmetry breaking in the many-body electronic states, appears in many Fe-based superconductors [1]. Above the structural transition temperature T_S, the electronic nematic susceptibility develops divergently, observed as the softening of shear modulus C_{66} [2,3], and the enhancements of the low-energy Raman spectrum [4,5] and in-plane anisotropy of resistivity $\Delta\rho$ [6]. The mechanism of nematicity and its order parameter attract increasing attention, as a key to understand the pairing mechanism of high-T_c superconductivity. The intimate relationship between nematicity and magnetism has been discussed based on the spin-nematic scenarios [7–14] and the orbital/charge-order scenarios [15–25].

Beyond the initial expectations, Fe-based superconductors exhibit very rich phase diagrams with nematicity and magnetism. In FeSe, for example, the nematic order does not accompany the magnetism at ambient pressure, whereas this nonmagnetic nematic phase is suppressed and replaced with the spin-density wave (SDW) phase by applying pressure [26,27]. This phase diagram is understood in terms of the orbital-order scenario by assuming the pressure-induced d_{xy}-orbital hole pocket [28]. In the orbital/charge-order scenario, the orbital/charge order is driven by the spin fluctuations, due to the Aslamazov-Larkin (AL) vertex correction (VC) that describes the charge-spin mode coupling. The significance of the AL process has been clarified by several theoretical studies, especially by renormalization group studies [25,29–33]. However, the origin of the diverse electronic states associated with charge, orbital, and spin degrees of freedom is not fully understood.

Until recently, all the discovered nematic orders in Fe-based superconductors have B_{1g} ($=d_{x^2-y^2}$) symmetry, along the nearest Fe-Fe direction. Recently, however, nematic order/fluctuation with B_{2g} ($=d_{xy}$) symmetry, rotated by 45° from the conventional B_{1g} nematicity, has been discovered in the heavily hole-doped ($n_d = 5.5$) compound AFe$_2$As$_2$ (A = Cs, Rb). Strong B_{2g} nematic fluctuations and static order have been discovered by the NMR study [34], the quasiparticle interference by scanning tunneling microscopy (STM) [35], and the measurement of in-plane anisotropy of resistivity [36] in RbFe$_2$As$_2$ ($T_c \sim 2.5$ K) and CsFe$_2$As$_2$ ($T_c \sim 1.8$ K). No SDW transition is observed in both compounds down to T_c [36,37]. Surprisingly, both B_{1g} and B_{2g} nematic transitions are observed in Y-based [38] and Hg-based [39] cuprate superconductors, respectively, at the pseudogap temperature T^*. Theoretical studies of nematicity in cuprates have been performed by many authors [29,40–47]. The discovery of unexpected B_{2g} nematicity in both Fe-based and cuprate superconductors puts a severe constraint on the mechanism of nematicity.

In this Rapid Communication, to reveal the origin of the B_{2g} nematicity, we study the spin-fluctuation-driven charge nematicity in AFe$_2$As$_2$ by considering the higher-order VCs. We predict that the "nematic bond order," given by the symmetry breaking in the d_{xy}-orbital correlated hopping, is responsible for the B_{2g} nematic order in AFe$_2$As$_2$. The Dirac pockets around the X, Y points play an essential role on the B_{2g} bond order. With electron doping, it is predicted that the B_{2g} nematicity changes to the conventional B_{1g} nematicity at the Lifshitz transition point, at which two Dirac pockets merge into one electron Fermi surface (FS). The diverse nematicity in A_{1-x}Ba$_x$Fe$_2$As$_2$ is naturally understood since the charge nematicity caused by the AL-VCs is sensitive to the orbital character and topology of the FS. The present study gives a great hint to control the nature of nematicity in Fe-based superconductors.

First, we introduce the nematic order parameters. Figure 1(a) shows B_{1g} nematic states due to orbital order ($n_{xz} \neq n_{yz}$). Here, the (x, y) axes are along the nearest Fe-Fe directions. The orbital order is the origin of the B_{1g} nematicity in Fe-based superconductors. Figure 1(b) shows the B_{2g} nematic state given by the next-nearest-neighbor (NNN) bond order, which corresponds to the modulation of the NNN correlated hopping δt_2. We propose that the B_{2g} bond order

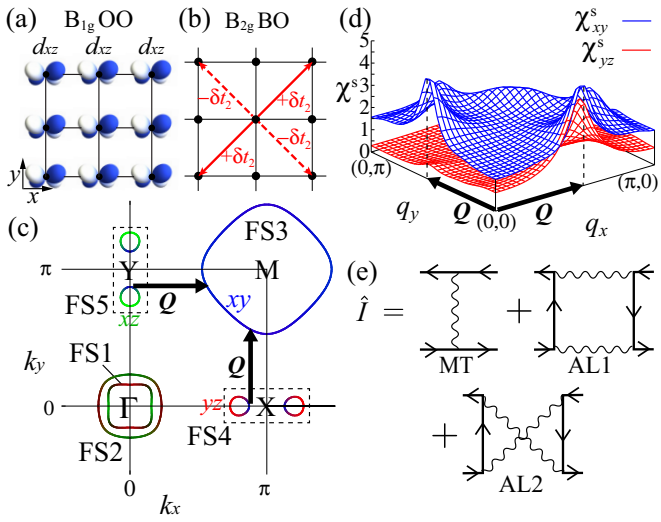

FIG. 1. Schematic pictures of (a) B_{1g} orbital order (OO), and (b) B_{2g} bond order (BO). (c) FSs of the $CsFe_2As_2$ model in unfolded zone. The colors green, red, and blue correspond to orbitals 2, 3, and 4, respectively. Each arrow denotes the significant intra-d_{xy}-orbital nesting vector $\boldsymbol{Q} = (0.53\pi, 0)$. (d) $\boldsymbol{q}$ dependences of $\chi^s_{xy}(\boldsymbol{q}, 0)$ and $\chi^s_{yz}(\boldsymbol{q}, 0)$ given by the RPA. (e) Feynman diagrams of the irreducible four-point vertex $\hat{I}$. The wavy line is the fluctuation-mediated interaction $\hat{V}^{s,c}$.

is the origin of the B_{2g} nematicity in AFe_2As_2, which has not been discussed in previous theoretical studies [23,41,43,44].

We analyze the following two-dimensional eight-orbital d-p Hubbard model with parameter r [20]:

$$H_{\rm M}(r) = H^0 + rH^U, \tag{1}$$

where H^0 is the unfolded tight-binding model derived from the first-principles calculation for $CsFe_2As_2$, which we introduce in the Supplemental Material (SM) A [48]. H^U is the first-principles screened Coulomb potential for d electrons in $BaFe_2As_2$ [49]. Figure 1(c) shows the FSs: The hole FS around the M point (FS3) composed of the d_{xy} orbital is large, while the Dirac pockets near the X and Y points (FS4,5) are small. The arrows denote the most important intra-d_{xy}-orbital nesting vectors. Below, we denote the five d orbitals $d_{3z^2-r^2}$, d_{xz}, d_{yz}, d_{xy}, and $d_{x^2-y^2}$ as $l = 1, 2, 3, 4, 5$.

We calculate the spin (charge) susceptibilities $\hat{\chi}^{s(c)}(q)$ for $q = (\boldsymbol{q}, \omega_m = 2m\pi T)$ based on the random-phase approximation (RPA). The spin Stoner factor α_s is given by the maximum eigenvalue of $\hat{\Gamma}^s\hat{\chi}^0(\boldsymbol{q}, 0)$, where $\hat{\Gamma}^{s(c)}$ is the bare Coulomb interaction for the spin (charge) channel, and $\hat{\chi}^0$ is the irreducible susceptibilities given by the Green's function without self-energy $\hat{G}(k) = [(i\epsilon_n - \mu)\hat{1} - \hat{h}^0(\boldsymbol{k})]^{-1}$ for $k = [\boldsymbol{k}, \epsilon_n = (2n+1)\pi T]$. Here, $\hat{h}^0(\boldsymbol{k})$ is the matrix expression of H^0 and μ is the chemical potential. Details of $\hat{\Gamma}^{s(c)}$, $\hat{\chi}^{s(c)}(q)$, and $\hat{\chi}^0(q)$ are explained in the SM A [48]. We use $N = 64 \times 64$ $\boldsymbol{k}$ meshes and 512 Matsubara frequencies, and fix the parameters $r = 0.30$ and $T = 0.03$ eV unless otherwise noted. Figure 1(d) shows the obtained spin susceptibility $\chi^s_{xy(yz)}(\boldsymbol{q}, 0) \equiv \chi^s_{l,l;l,l}(\boldsymbol{q}, 0)$ with $l = 4$ ($l = 3$) at $\alpha_s = 0.93$. χ^s_{xy} is enlarged due to the intra-d_{xy}-orbital nesting, and it has the largest peak at $\boldsymbol{q} = \boldsymbol{Q} = (0.53\pi, 0)$. In contrast, χ^s_{yz} is small since the intra-d_{yz}-orbital nesting is bad. Note that $\chi^s_{xy} \leqslant \chi^s_{yz}$ in LaFeAsO, $BaFe_2As_2$, and FeSe since two Dirac pockets (FS4 and FS5) merge into a usual electron pocket for $n_d \sim 6.0$.

Hereafter, we study the symmetry breaking in the self-energy ($\Delta\hat{\Sigma}$) based on the density-wave (DW) equation introduced in Ref. [20]. We calculate both momentum and orbital dependences of $\Delta\Sigma^{\boldsymbol{q}}_{l,l'}(k)$ self-consistently in order to analyze both orbital order and bond order on equal footing. To find the wave vector $\boldsymbol{q}$ of the DW state, we solve the following linearized DW equation:

$$\lambda_{\boldsymbol{q}}\Delta\hat{\Sigma}^{\boldsymbol{q}}(k) = \frac{T}{N}\sum_{k'}\hat{K}^{\boldsymbol{q}}(k,k')\Delta\hat{\Sigma}^{\boldsymbol{q}}(k'), \tag{2}$$

where $\lambda_{\boldsymbol{q}}$ is the eigenvalue for the DW equation. The DW with wave vector $\boldsymbol{q}$ appears when $\lambda_{\boldsymbol{q}} = 1$, and the eigenvector $\Delta\hat{\Sigma}^{\boldsymbol{q}}(k)$ gives the DW form factor. The kernel function $\hat{K}^{\boldsymbol{q}}(k,k')$ [40] is given by

$$\hat{K}^{\boldsymbol{q}}(k,k') = \hat{I}^{\boldsymbol{q}}(k,k')\hat{g}^{\boldsymbol{q}}(k'), \tag{3}$$

where $g^{\boldsymbol{q}}_{l,l';m,m'}(k) \equiv G_{l,m}(k + \frac{q}{2})G_{m',l'}(k - \frac{q}{2})$, and $\hat{I}^{\boldsymbol{q}}(k,k')$ is the irreducible four-point vertex. It is given by the Ward identity $\hat{I} = \delta\hat{\Sigma}/\delta\hat{G}$, where $\hat{\Sigma}$ is one-loop self-energy [50]. The Feynman diagram of $\hat{I}^{\boldsymbol{q}}$ is shown in Fig. 1(e): The first diagram corresponds to the Maki-Thompson (MT) term, and the second and the third diagrams are AL1 and AL2 terms, respectively. Its analytic expression is given in SM A [48]. Near the magnetic criticality, the charge-channel interaction due to the AL terms is strongly enhanced in proportion to $\sum_p\{\chi^s(\boldsymbol{p}, 0)\}^2$, which is proportional to $\chi^s(\boldsymbol{Q}, 0)$ in two-dimensional systems. For this reason, the AL terms cause the spin-fluctuation-driven charge nematic order [18,20,29–31].

The Hartree-Fock (HF) term, which is the first-order term with respect to $\hat{\Gamma}^{s,c}$, is included in the MT term. As well known, the HF term suppresses conventional charge DW order ($\Delta\Sigma = \text{const}$), whereas both B_{1g} and B_{2g} bond orders are not suppressed. Here, we drop the ϵ_n dependence of $\Delta\hat{\Sigma}^{\boldsymbol{q}}(k)$ by the analytic continuation ($\epsilon_n \to \epsilon$) and putting $\epsilon = 0$ [20]. This approximation leads to slight overestimation of $\lambda_{\boldsymbol{q}}$.

Figures 2(a) and 2(b) show the obtained form factors at $\boldsymbol{q} = \boldsymbol{0}$, $\Delta\Sigma^{\boldsymbol{0}}_4(\boldsymbol{k}) \equiv \Delta\Sigma^{\boldsymbol{0}}_{4,4}(\boldsymbol{k})$, and $\Delta\Sigma^{\boldsymbol{0}}_3(\boldsymbol{k}) \equiv \Delta\Sigma^{\boldsymbol{0}}_{3,3}(\boldsymbol{k})$, for the largest eigenvalue $\lambda = 0.93$. (The absolute value of $\Delta\hat{\Sigma}^{\boldsymbol{q}}$ is meaningless.) The obtained form factor has B_{2g} symmetry since the symmetry relation $\Delta\Sigma^{\boldsymbol{0}}_4(k_x, k_y) \propto \sin k_x \sin k_y$ holds. The relation $|\Delta\Sigma_{xy}| \gg |\Delta\Sigma_{yz(xz)}|$ means that the primary nematic order is the "next-nearest-neighbor bond order for d_{xy} orbital," which is shown in Fig. 1(b). The obtained B_{2g} bond order is consistent with the experimental B_{2g} nematicity in AFe_2As_2 [34–36]. The second largest eigenvalue $\lambda = 0.88$ corresponds to the B_{1g} nematic bond order, the details of which we explain in SM B [48].

As explained in SM C [48], the nematic susceptibility with respect to the form factor $\Delta\hat{\Sigma}^{\boldsymbol{q}}$ is given as $\hat{\chi}^{\Delta\Sigma}(\boldsymbol{q}) \propto (1 - \lambda_{\boldsymbol{q}})^{-1}$ that diverges at $\lambda_{\boldsymbol{q}} = 1$. Figure 2(c) shows the T dependences of $(1 - \lambda_{\boldsymbol{0}})^{-1}$ for both B_{2g} and B_{1g} symmetry solutions. We see that $(1 - \lambda_{\boldsymbol{0}})^{-1}$ for the B_{2g} symmetry shows the Curie-Weiss behavior and dominates over that for the B_{1g} symmetry. These results are consistent with the experimental nematic susceptibility [34,36]. In Fig. 2(d), we show the

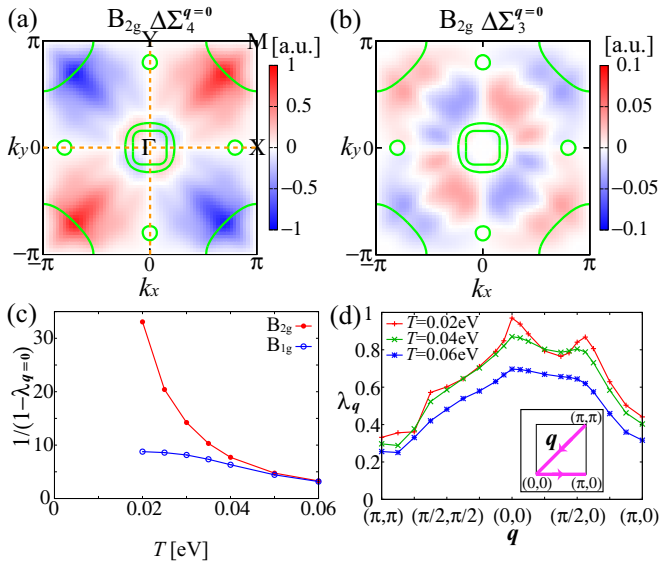

FIG. 2. (a), (b) B_{2g} symmetry form factors at $\boldsymbol{q} = \boldsymbol{0}$ obtained as the largest eigenvalue. The primary form factor on the d_{xy} orbital, $\Delta\Sigma_4^{\boldsymbol{0}} \propto \sin k_x \sin k_y$, gives the bond order. Orange dotted lines represent the symmetry nodes. (c) The strengths of nematic fluctuations $1/(1-\lambda_{\boldsymbol{q}=\boldsymbol{0}})$ for B_{2g} and B_{1g} symmetries as a function of T. (d) $\boldsymbol{q}$ dependences of the maximum eigenvalue at $T = 0.02$, 0.04, and 0.06 eV.

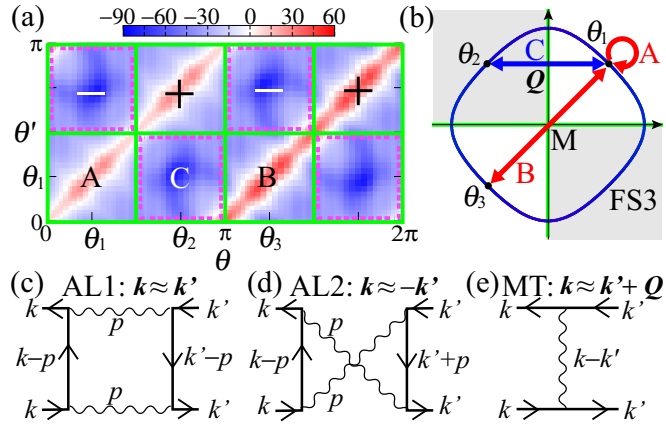

FIG. 3. (a) $K_{\mathrm{FS3}}(\theta, \theta')$ on FS3 given by all vertex terms. The green lines denote the B_{2g} symmetry nodes. A, B, and C represent the pairs of Fermi points (θ_1, θ_1), (θ_3, θ_1), and (θ_2, θ_1), respectively: $\theta_1 \equiv \pi/4$, $\theta_2 \equiv 3\pi/4$, and $\theta_3 \equiv 5\pi/4$. (b) B_{2g} symmetry order $[\Delta\Sigma(\boldsymbol{k}) \propto \sin k_x \sin k_y]$ driven by attractive (repulsive) interaction for pairs A and B (pair C). (c)–(e) $\hat{I}^{\boldsymbol{0}}(k, k')$ given by AL1 term, AL2 term, and MT term. Two AL terms give a strong attractive interaction for $(\boldsymbol{k}, \pm\boldsymbol{k})$, shown as red line regions in panel (a). The MT gives a repulsive interaction for pair C, due to spin fluctuations at $\boldsymbol{Q} \approx (0.5\pi, 0)$.

$\boldsymbol{q}$ dependences of the largest eigenvalue at $T = 0.02$, 0.04, and 0.06 eV. It is confirmed that the nematic susceptibility actually has the maximum peak at $\boldsymbol{q} = \boldsymbol{0}$, and the symmetry of form factor is B_{2g}.

In order to understand the origin of the B_{2g} nematic bond order, we analyze the momentum dependence of the kernel function for the d_{xy} orbital. Figure 3(a) shows $K_{\mathrm{FS3}}(\theta, \theta') \equiv T\sum_{n'} K^{\boldsymbol{0}}_{4,4;4,4}(\boldsymbol{k}(\theta), \epsilon_n, \boldsymbol{k}(\theta'), \epsilon_{n'})|_{\epsilon_n \to 0}$ given by the summation of the AL1, AL2, and MT terms on the FS3. Here, θ and θ' denote the azimuthal angles (from the M point) of $\boldsymbol{k}$ and $\boldsymbol{k}'$ on the FS3, respectively. Now, we define the pairs of Fermi points $\mathrm{A} = (\theta_1, \theta_1)$, $\mathrm{B} = (\theta_3, \theta_1)$, and $\mathrm{C} = (\theta_2, \theta_1)$, where $\theta_1 \equiv \pi/4$, $\theta_2 \equiv 3\pi/4$, and $\theta_3 \equiv 5\pi/4$. For these pairs $K_{\mathrm{FS3}}(\theta, \theta')$ becomes large in magnitude. The green lines denote the nodes of B_{2g} symmetry $(\theta, \theta' = \frac{\pi}{2}n)$. The positive $K_{\mathrm{FS3}}(\theta, \theta')$ for the pairs A and B give attractive interactions between the same $(\boldsymbol{k}_1, \boldsymbol{k}_1)$ and the opposite $(-\boldsymbol{k}_1, \boldsymbol{k}_1)$ momenta in Eq. (2), respectively, where $\boldsymbol{k}_i \equiv \boldsymbol{k}(\theta_i)$ $(i = 1, 2, 3)$. On the other hand, the negative $K_{\mathrm{FS3}}(\theta, \theta')$ for the pair C gives the repulsive interaction between $(\boldsymbol{k}_2, \boldsymbol{k}_1)$. As we show in Fig. 3(b), this checkerboard-type sign structure of $K_{\mathrm{FS3}}(\theta, \theta')$, which is positive (negative) for pairs A and B (pair C), favors the B_{2g} symmetry bond order $\Delta\Sigma_4^{\boldsymbol{0}}(\boldsymbol{k}) \propto \sin k_x \sin k_y$.

We briefly explain the microscopic origin of the checkerboard-type sign structure in $K_{\mathrm{FS3}}(\theta, \theta')$. The positive $K_{\mathrm{FS3}}(\theta, \theta')$ along $\theta' = \theta$ in Fig. 3(a) (including the pair A) originates from the AL1 term, since the particle-hole channel $\phi_{\mathrm{p\text{-}h}} \equiv T\sum_p G_{4,4}(k-p)G_{4,4}(k'-p)$ shown in Fig. 3(c) takes a large positive value for $\boldsymbol{k}' = \boldsymbol{k}$, as we explain in SM D [48]. Also, the positive $K_{\mathrm{FS3}}(\theta, \theta')$ along $\theta' = \theta + \pi$ (including the pair B) originates from the AL2 term, since the particle-particle (Cooper) channel $\phi_{\mathrm{p\text{-}p}} \equiv T\sum_p G_{4,4}(k-p)G_{4,4}(k'+p)$ shown in Fig. 3(d) takes a large positive value for $\boldsymbol{k}' = -\boldsymbol{k}$. On the other hand, the negative $K_{\mathrm{FS3}}(\theta_2, \theta_1)$ at the pair C stems from the MT term in Fig. 3(e). This is because $\hat{V}^s(k-k') \propto \hat{\chi}^s(k-k')$ in the MT term becomes maximum for $(\boldsymbol{k}, \boldsymbol{k}') = (\boldsymbol{k}_2, \boldsymbol{k}_1)$ since $\boldsymbol{k}_2 - \boldsymbol{k}_1$ coincides with the nesting vector $\boldsymbol{Q}$.

To summarize, both B_{1g} and B_{2g} nematicities can be induced by the AL terms, since they give attractive interaction for both $\theta \approx \theta'$ and $\theta \approx \theta' + \pi$. In fact, both the nematic susceptibilities $(1-\lambda_{\boldsymbol{q}})^{-1}$ for the B_{1g} and the B_{2g} increase as shown in Fig. 2(c), consistently with recent experiment [36]. In the present model with spin fluctuations at $\boldsymbol{Q} \approx (0.5\pi, 0)$, the B_{2g} nematic order is assisted by the MT term. The magnitude of the AL kernel function dominates over that of the MT kernel function as we explain in SM D [48]. For this reason, the eigenvalue of the DW equation $\lambda_{\boldsymbol{q}}$ can be larger than that of the Eliashberg gap equation, in which the kernel contains only the MT term [51]. We predict that the B_{2g} nematicity is closely tied to the Dirac pockets, which give the main spin fluctuations in $A\mathrm{Fe}_2\mathrm{As}_2$.

Here, we discuss the doping dependence of the nematicity: We introduce a reliable model Hamiltonian for $\mathrm{Cs}_{1-x}\mathrm{Ba}_x\mathrm{Fe}_2\mathrm{As}_2$, by interpolating between the $\mathrm{CsFe}_2\mathrm{As}_2$ model and the $\mathrm{BaFe}_2\mathrm{As}_2$ model with the ratio $1-x : x$. With increasing x, the FSs with four Dirac pockets in Fig. 4(a) for $x = 0.4$ change to the FSs with two electron pockets in Fig. 4(b) for $x = 0.6$. In this model, the Lifshitz transition occurs at $x_c \approx 0.5$.

Figure 4(c) shows x dependences of $\lambda_{\boldsymbol{q}=\boldsymbol{0}}$ for the B_{2g} and the B_{1g} symmetries in the $\mathrm{Cs}_{1-x}\mathrm{Ba}_x\mathrm{Fe}_2\mathrm{As}_2$ model, in which the value of r is fixed to 0.30. For $x < x_c$, the B_{2g} bond order $\pm\delta t_2$ shown in Fig. 1(b) is dominant over the B_{1g} orbital order, since the former is driven by strong spin fluctuations in the d_{xy}

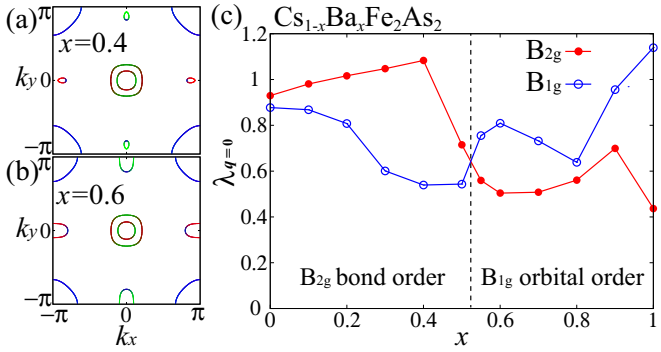

FIG. 4. (a) FSs for $x = 0.4$ and (b) FSs for $x = 0.6$ in the $Cs_{1-x}Ba_xFe_2As_2$ model. (c) x dependences of λ for B_{2g} and B_{1g} symmetry obtained in the $Cs_{1-x}Ba_xFe_2As_2$ model.

orbital. For $x > x_c$, the B_{1g} orbital order $n_{xz} \neq n_{yz}$ in Fig. 1(a) becomes dominant, because of the strong spin fluctuations in the $d_{xz,yz}$ orbitals due to the nesting between electron and hole FSs [18,19,21], as we briefly explain in SM E [48]. Thus, the present theory naturally explains both the B_{1g} nematicity in nondoped ($n_d \approx 6$) systems and the B_{2g} nematicity in heavily hole-doped compounds in a unified way, by focusing on the impact of the Lifshitz transition.

The sudden decrease of $\lambda_{\boldsymbol{0}}^{B_{2g}}$ at the Lifshitz transition point in Fig. 4(c) indicates that the Dirac pockets are essential for the B_{2g} nematicity, in spite of their small size. To verify this, we calculate $\chi^s_{xy}(q)$ by dropping the contribution from the rectangular areas around the X, Y points shown in Fig. 1(c): Then, as shown in Fig. 5(a), the peak at $\boldsymbol{Q} = (0.53\pi, 0)$ of $\chi^s_{xy}(q)$ in Fig. 1(d) shifts to $\boldsymbol{Q}' = (0.56\pi, 0.56\pi)$, which is the intra-FS3 nesting vector. In this case, $K_{\rm FS3}(\theta, \theta')$ due to the MT term takes a large negative value for $\theta \approx \theta_a$ and $\theta' \approx \theta'_a$ in Fig. 5(b), and therefore B_{1g} bond order emerges: $\lambda_{\boldsymbol{0}}^{B_{1g}} = 0.82$ and $\lambda_{\boldsymbol{0}}^{B_{2g}} = 0.77$. To summarize, the B_{2g} nematicity in AFe_2As_2 is closely tied to the emergence of the Dirac pockets at the Lifshitz transition. Thus, we can control the nematicity by changing the topology and orbital character of the FSs.

Recently, the B_{2g} vestigial nematic order has been proposed in Refs. [52,53] based on the real-space picture, whereas the double stripe magnetism [$\boldsymbol{q} = (\pi/2, \pi/2)$] has not been observed yet. Thus, it is an important future issue to determine the mechanism of B_{2g} nematicity.

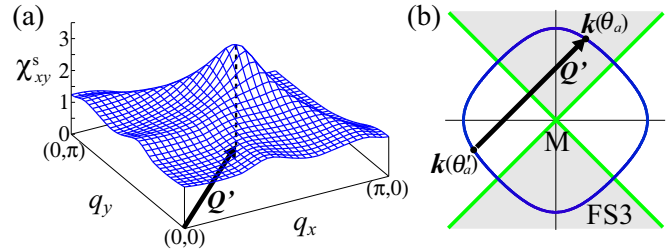

FIG. 5. (a) $\chi^s_{xy}(q)$ for $r = 0.36$ ($\alpha_S = 0.90$) given by dropping the contribution from the Dirac pockets. (b) B_{1g} nematic order with green symmetry nodes and gray negative region on FS3 due to the intra-FS nesting $\boldsymbol{Q}' \approx (0.6\pi, 0.6\pi)$.

In summary, we studied the rich variety of nematic orders realized in $A_{1-x}Ba_xFe_2As_2$ (A = Cs, Rb) by solving the DW equation with AL- and MT-VCs. At $x = 0$, the B_{2g} bond order is driven by the spin fluctuations in the d_{xy} orbital. With increasing x, the B_{2g} nematicity suddenly changes to B_{1g} orbital nematicity ($n_{xz} - n_{yz}$) at the Lifshitz transition point, consistently with recent experiment [36]. Both the FS orbital character and the FS topology are key ingredients not only to understand the diverse nematicity, but also to control the nature of nematicity in Fe-based superconductors. The present theory will give useful hints to understand recently discovered rich nematic orders in cuprate superconductors [38,39].

We stress that the present DW equations satisfy the criteria of the "conserving approximation (CA)" by introducing the self-energy in G's [54–56]. The great merit of the CA is that the macroscopic conservation laws are satisfied rigorously. This merit is important to avoid unphysical results. In SM F [48], we improve the present theory within the framework of the CA, by introducing the self-energy given by the fluctuation-exchange approximation. The obtained $\boldsymbol{q}$ dependences of $\lambda_{\boldsymbol{q}}$ and B_{2g} symmetry form factor are essentially similar to Fig. 2. Thus, the main results of the present study are justified within the framework of the CA.

We are grateful to Y. Matsuda, T. Shibauchi, and Y. Yamakawa for useful discussions. This work was supported by the "Quantum Liquid Crystals" No. JP19H05825 KAKENHI on Innovative Areas from JSPS of Japan, and JSPS KAKENHI (No. JP17K05543).

[1] M. Yi, D. H. Lu, J.-H. Chu, J. G. Analytis, A. P. Sorini, A. F. Kemper, B. Moritz, S.-K. Mo, R. G. Moore, M. Hashimoto, W.-S. Lee, Z. Hussain, T. P. Devereaux, I. R. Fisher, and Z.-X. Shen, Proc. Natl. Acad. Sci. USA **108**, 6878 (2011).

[2] M. Yoshizawa, D. Kimura, T. Chiba, S. Simayi, Y. Nakanishi, K. Kihou, C.-H. Lee, A. Iyo, H. Eisaki, M. Nakajima, and S. Uchida, J. Phys. Soc. Jpn. **81**, 024604 (2012).

[3] A. E. Böhmer, P. Burger, F. Hardy, T. Wolf, P. Schweiss, R. Fromknecht, M. Reinecker, W. Schranz, and C. Meingast, Phys. Rev. Lett. **112**, 047001 (2014).

[4] Y. Gallais, R. M. Fernandes, I. Paul, L. Chauviere, Y.-X. Yang, M.-A. Measson, M. Cazayous, A. Sacuto, D. Colson, and A. Forget, Phys. Rev. Lett. **111**, 267001 (2013).

[5] Y. Hu, X. Ren, R. Zhang, H. Luo, S. Kasahara, T. Watashige, T. Shibauchi, P. Dai, Y. Zhang, Y. Matsuda, and Y. Li, Phys. Rev. B **93**, 060504(R) (2016).

[6] J.-H. Chu, H.-H. Kuo, J. G. Analytis, and I. R. Fisher, Science **337**, 710 (2012).

[7] R. M. Fernandes, L. H. VanBebber, S. Bhattacharya, P. Chandra, V. Keppens, D. Mandrus, M. A. McGuire, B. C. Sales, A. S. Sefat, and J. Schmalian, Phys. Rev. Lett. **105**, 157003 (2010).

[8] F. Wang, S. A. Kivelson, and D.-H. Lee, Nat. Phys. **11**, 959 (2015).

[9] R. Yu and Q. Si, Phys. Rev. Lett. **115**, 116401 (2015).

[10] J. K. Glasbrenner, I. I. Mazin, H. O. Jeschke, P. J. Hirschfeld, and R. Valenti, Nat. Phys. **11**, 953 (2015).

[11] C. Fang, H. Yao, W.-F. Tsai, J. P. Hu, and S. A. Kivelson, Phys. Rev. B **77**, 224509 (2008).

[12] R. M. Fernandes and A. V. Chubukov, Rep. Prog. Phys. **80**, 014503 (2017).

[13] A. E. Böhmer, F. Hardy, L. Wang, T. Wolf, P. Schweiss, and C. Meingast, Nat. Commun. **6**, 7911 (2015).

[14] R. Khasanov, R. M. Fernandes, G. Simutis, Z. Guguchia, A. Amato, H. Luetkens, E. Morenzoni, X. Dong, F. Zhou, and Z. Zhao, Phys. Rev. B **97**, 224510 (2018).

[15] F. Krüger, S. Kumar, J. Zaanen, and J. van den Brink, Phys. Rev. B **79**, 054504 (2009).

[16] W. Lv, J. Wu, and P. Phillips, Phys. Rev. B **80**, 224506 (2009).

[17] C.-C. Lee, W.-G. Yin, and W. Ku, Phys. Rev. Lett. **103**, 267001 (2009).

[18] S. Onari and H. Kontani, Phys. Rev. Lett. **109**, 137001 (2012).

[19] S. Onari, Y. Yamakawa, and H. Kontani, Phys. Rev. Lett. **112**, 187001 (2014).

[20] S. Onari, Y. Yamakawa, and H. Kontani, Phys. Rev. Lett. **116**, 227001 (2016).

[21] Y. Yamakawa, S. Onari, and H. Kontani, Phys. Rev. X **6**, 021032 (2016).

[22] S. Onari and H. Kontani, in *Iron-Based Superconductivity*, edited by P. D. Johnson, G. Xu, and W.-G. Yin (Springer-Verlag, Berlin, Heidelberg, 2015).

[23] K. Jiang, J. Hu, H. Ding, and Z. Wang, Phys. Rev. B **93**, 115138 (2016).

[24] L. Fanfarillo, G. Giovannetti, M. Capone, and E. Bascones, Phys. Rev. B **95**, 144511 (2017).

[25] A. V. Chubukov, M. Khodas, and R. M. Fernandes, Phys. Rev. X **6**, 041045 (2016).

[26] K. Kothapalli, A. E. Böhmer, W. T. Jayasekara, B. G. Ueland, P. Das, A. Sapkota, V. Taufour, Y. Xiao, E. Alp, S. L. Budko, P. C. Canfield, A. Kreyssig, and A. I. Goldman, Nat. Commun. **7**, 12728 (2016).

[27] J. P. Sun, K. Matsuura, G. Z. Ye, Y. Mizukami, M. Shimozawa, K. Matsubayashi, M. Yamashita, T. Watashige, S. Kasahara, Y. Matsuda, J.-Q. Yan, B. C. Sales, Y. Uwatoko, J.-G. Cheng, and T. Shibauchi, Nat. Commun. **7**, 12146 (2016).

[28] Y. Yamakawa and H. Kontani, Phys. Rev. B **96**, 144509 (2017).

[29] M. Tsuchiizu, K. Kawaguchi, Y. Yamakawa, and H. Kontani, Phys. Rev. B **97**, 165131 (2018).

[30] M. Tsuchiizu, Y. Ohno, S. Onari, and H. Kontani, Phys. Rev. Lett. **111**, 057003 (2013).

[31] M. Tsuchiizu, Y. Yamakawa, and H. Kontani, Phys. Rev. B **93**, 155148 (2016).

[32] R.-Q. Xing, L. Classen, and Andrey V. Chubukov, Phys. Rev. B **98**, 041108(R) (2018).

[33] U. Karahasanovic, F. Kretzschmar, T. Bohm, R. Hackl, I. Paul, Y. Gallais, and J. Schmalian, Phys. Rev. B **92**, 075134 (2015).

[34] J. Li, D. Zhao, Y. P. Wu, S. J. Li, D. W. Song, L. X. Zheng, N. Z. Wang, X. G. Luo, Z. Sun, T. Wu, and X. H. Chen, arXiv:1611.04694.

[35] X. Liu, R. Tao, M. Ren, W. Chen, Q. Yao, T. Wolf, Y. Yan, T. Zhang, and D. Feng, Nat. Commun. **10**, 1039 (2019).

[36] K. Ishida, M. Tsujii, S. Hosoi, Y. Mizukami, S. Ishida, A. Iyo, H. Eisaki, T. Wolf, K. Grube, H. V. Löhneysen, R. M. Fernandes, and T. Shibauchi, arXiv:1812.05267.

[37] Y. P. Wu, D. Zhao, A. F. Wang, N. Z. Wang, Z. J. Xiang, X. G. Luo, T. Wu, and X. H. Chen, Phys. Rev. Lett. **116**, 147001 (2016).

[38] Y. Sato, S. Kasahara, H. Murayama, Y. Kasahara, E.-G. Moon, T. Nishizaki, T. Loew, J. Porras, B. Keimer, T. Shibauchi, and Y. Matsuda, Nat. Phys. **13**, 1074 (2017).

[39] H. Murayama, Y. Sato, R. Kurihara, S. Kasahara, Y. Mizukami, Y. Kasahara, H. Uchiyama, A. Yamamoto, E.-G. Moon, J. Cai, J. Freyermuth, M. Greven, T. Shibauchi, and Y. Matsuda, arXiv:1805.00276.

[40] K. Kawaguchi, M. Tsuchiizu, Y. Yamakawa, and H. Kontani, J. Phys. Soc. Jpn. **86**, 063707 (2017).

[41] S. Sachdev and R. La Placa, Phys. Rev. Lett. **111**, 027202 (2013).

[42] E. Fradkin, S. A. Kivelson, and J. M. Tranquada, Rev. Mod. Phys. **87**, 457 (2015).

[43] C. Husemann and W. Metzner, Phys. Rev. B **86**, 085113 (2012).

[44] C. J. Halboth and W. Metzner, Phys. Rev. Lett. **85**, 5162 (2000).

[45] Y. Yamakawa and H. Kontani, Phys. Rev. Lett. **114**, 257001 (2015).

[46] P. A. Lee, Phys. Rev. X **4**, 031017 (2014).

[47] X. Montiel, T. Kloss, and C. Pépin, Phys. Rev. B **95**, 104510 (2017).

[48] See Supplemental Material at http://link.aps.org/supplemental/10.1103/PhysRevB.100.020507 for the nematic susceptibility, details of the kernel function, origin of B_{1g} orbital order, and conserving approximation.

[49] T. Miyake, K. Nakamura, R. Arita, and M. Imada, J. Phys. Soc. Jpn. **79**, 044705 (2010).

[50] The one-loop (single-fluctuation-exchange) self-energy is given by $\hat{\Sigma}(k) = \frac{T}{N}\sum_q \hat{V}^{\Sigma}(q)\hat{G}(k-q)$, where $\hat{V}^{\Sigma} = \frac{3}{2}\hat{\Gamma}^s\hat{\chi}^s(q)\hat{\Gamma}^s + \frac{1}{2}\hat{\Gamma}^c\hat{\chi}^c(q)\hat{\Gamma}^c - \frac{1}{2}[\hat{\Gamma}^c\hat{\chi}^0(q)\hat{\Gamma}^c + \hat{\Gamma}^s\hat{\chi}^0(q)\hat{\Gamma}^s - \frac{1}{4}(\hat{\Gamma}^s + \hat{\Gamma}^c)\hat{\chi}^0(q)(\hat{\Gamma}^s + \hat{\Gamma}^c)]$.

[51] V. Mishra and M. R. Norman, Phys. Rev. B **92**, 060507(R) (2015).

[52] V. Borisov, R. M. Fernandes, and R. Valenti, arXiv:1902.10729.

[53] Y. Wang, W. Hu, and Q. Si, arXiv:1903.00375.

[54] G. Baym and L. P. Kadanoff, Phys. Rev. **124**, 287 (1961).

[55] G. Baym and L. P. Kadanoff, Phys. Rev. **127**, 1391 (1962).

[56] H. Kontani, Rep. Prog. Phys. **71**, 026501 (2008).